OPEN

Image Decoding of Photonic Crystal Beads Array in the Microfluidic Chip for Multiplex Assays

Junjie Yuan[1,2], Xiangwei Zhao[1,2], Xiaoxia Wang[1,2] & Zhongze Gu[1,2]

[1]State Key Laboratory of Bioelectronics, School of Biological Science and Medical Engineering, Southeast University, Nanjing, 210096, China, [2]Laboratory of Environment and Biosafety Research Institute of Southeast University in Suzhou, Suzhou 215123, China.

Correspondence and requests for materials should be addressed to X.Z. (xwzhao@seu. edu.cn) or Z.G. (gu@ seu.edu.cn)

Along with the miniaturization and intellectualization of biomedical instruments, the increasing demand of health monitoring at anywhere and anytime elevates the need for the development of point of care testing (POCT). Photonic crystal beads (PCBs) as one kind of good encoded microcarriers can be integrated with microfluidic chips in order to realize cost-effective and high sensitive multiplex bioassays. However, there are difficulties in analyzing them towards automated analysis due to the characters of the PCBs and the unique detection manner. In this paper, we propose a strategy to take advantage of automated image processing for the color decoding of the PCBs array in the microfluidic chip for multiplex assays. By processing and alignment of two modal images of epi-fluorescence and epi-white light, every intact bead in the image is accurately extracted and decoded by PC colors, which stand for the target species. This method, which shows high robustness and accuracy under various configurations, eliminates the high hardware requirement of spectroscopy analysis and user-interaction software, and provides adequate supports for the general automated analysis of POCT based on PCBs array.

Molecular diagnostics plays a critical role in the prevention, identification and prognosis of disease. Since the 19th century a large number of molecules has been identified and studied to characterize the health of patients. And tremendous advances in the instrumental analysis including of both hardware and software have result in accurate and precise molecular detections with high degree of automation. However, most of the instruments are huge in volume and high in cost, which limited them to the central labs of hospitals especially in the developing countries. This situation is not in line with the direction of future health monitoring, for which highly accessible information acquisition tools and networks are the dominated features.

In this context, the research community of biomedical detection now has turned to the development of more portable, digital and intelligent instruments or devices, especially with the rapid development of microfluidic chip technology[1–5]. A recent manifestation of this potential is the emergence and rapid expansion of point of care testing (POCT), the aim of which is to provide healthcare services at the right point or place with quick response[6–11]. Although there is not much demand on the throughput of samples in POCT, multiplex and multi-functionality test are obviously the favorite assay formats in the real assays. However, to integrate such functional modules with microfluidic chips is challenging not only because of the consideration of cost but also the flexibility. As an example, there are limited reports on multiplex assays in POCT.

Photonic crystal beads (PCBs) assembled from monodispersed nanoparticles show stable colors derived from photonic bandgap (PBG) of 3D photonic crystal. And they were used to encode biomolecular carriers in multiplex bioassays with their reflection peak positions or colors as the encoding elements[12]. In comparison with fluor-escence encoding elements[13,14], the photonic crystal color or reflection peak is much more stable and does not suffer from fluorescence interference, bleaching and quenching[15–18]. At the same time, PCBs can be easily incorporated into microfluidic chips just by injection or vacuum. Although they are randomly distributed, their codes can be recognized by their reflection peaks, making multiplex assays in microfluidic chip more cost-effective and practical in realization. However, the reflection spectra of PCBs can only be measured on single bead of tens of microns in order to get its unique code[19], which means that high-cost microscopic spectrometer is needed. This greatly reduces the throughput of detection and makes it not realistic in practice considering the automated locating and measuring in the scenario of POCT.

Image analysis is intuitive and widely adapted in the microfluidic chip analysis recently owing to the miniaturization and low-cost of cameras[20–24]. Since the high throughput information acquired by imaging, it is believed that image collection and analysis will have a great impact on the development of portable and intelligent POCT systems. In this paper, we proposed to take advantage of image processing for the automated decoding and detection of PCBs array in microfluidic chip instead of spectral analysis. By this means, the high-precision positioning and scanning apparatuses needed for spectra acquisition of arrayed PCBs are excluded and hence the cost of analysis can be reduced.

As illustrated in Fig. 1 (a), a simple microfluidic chip with six parallel channels was designed and fabricated with flow-through reaction cells, in which the PCBs were introduced and trapped in a metal microchannel array. In application, the sample flows through the metal microchannels and reacts with probes molecules immobilized on the surface of PCBs array. Usually fluorescence labels are adopted to visualize the reaction result as in protein or DNA microarrays. The concentration of the analytes can be represented by fluorescence intensity of the PCBs. And by retrieving the color codes of these PCBs, the analytes categories can be identified. Hence an epi-fluorescence and epi-white light image are collected from the bottom of the reaction cell as detection and encoding image respectively (Fig. 1 (b) and (c)) in order to get the final result of the multiplex assays.
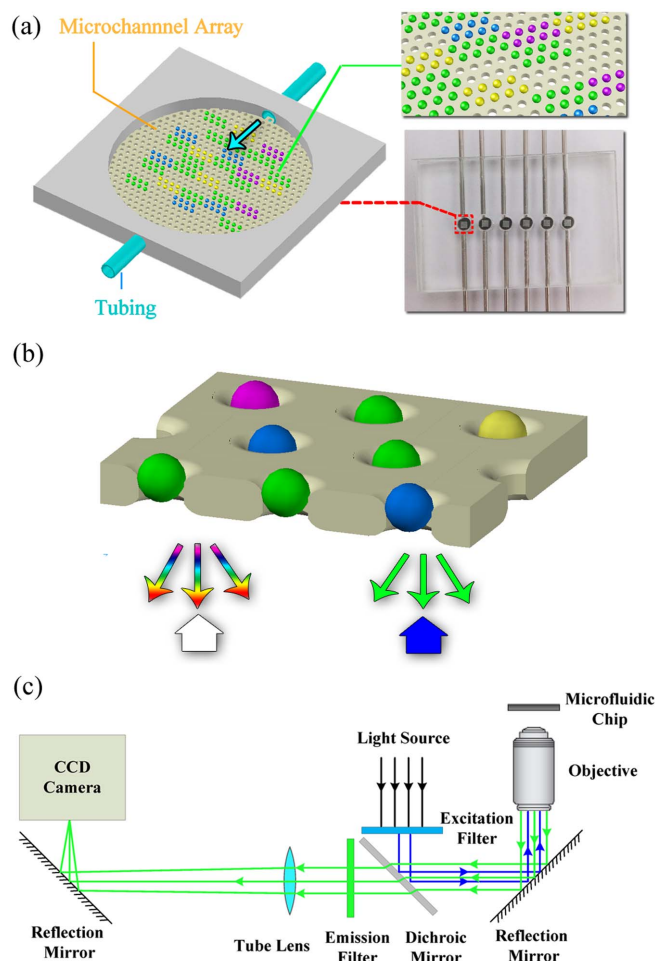
Unlike in conventional DNA/protein microarray, or fluorescence encoding based xMAP technology of Luminex Corporation, where only one or two fluorescence images of single modality are analyzed[25], there are two images of different modalities needed to be aligned and processed for the PCBs in the microfluidic cell. And the scattering of the metal microchannel array is very high whether illuminated with white light or excitation light (Fig. 2). What's more, the structure color of PCBs is iridescence since the angel-dependent reflection of photonic crystal[19,26]. All these characters blur the boundaries of objects and dissolve the colors of the PCBs, which imposed great difficulties in the process of image decoding and detection.

In our work, the epi-fluorescence image is firstly enhanced to increase the contrast. Subsequently, every intact bead is extracted with its boundary accurately determined. Then we employ a code identification algorithm to extract the characteristic colors from the iridescent beads and use a gating strategy to identify the different color codes in the epi-white light image. This method presents high accuracy even under different configurations, providing adequate supports for multiplex assays.

Results

Microfluidic chip and image acquisition of PCBs array. A transparent 3D microfluidic chip with six reaction cells of 2 mm diameter is shown in Fig. 1(a). In each reaction cell, there is a metal microchannel array as a trap for PCBs. And all the cells are connected with inlet and outlet channel from the upside and downside of the metal microchannel array. The diameter of one circular microchannel and PCB is 50 μm and 60 μm respectively. This microchannel array design guarantees the flow through reaction, and separates beads from each other, which avoids the fluorescence interference between adjacent beads. And rectangle microchannel array with side length of 40 μm is also used for further validation.

A home-constructed inverted optical microscopic detection system is illustrated in Fig. 1 (c) with coaxial illumination for epi-fluorescence and epi-white imaging. In the current setup, about 150 intact beads are able to be imaged in the field view. The images are saved in
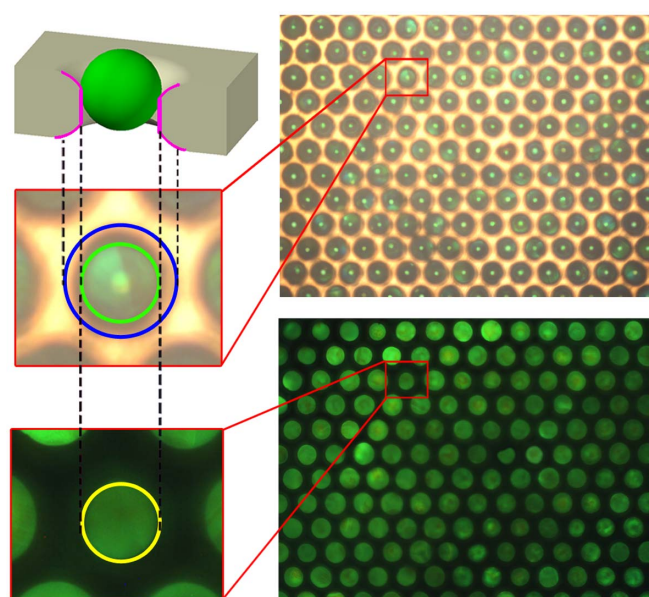

Figure 1 | PCBs array in a microfluidic chip and its image acquisition.
(a) The flow through microfluidic chip and the 3D illustrated structure of the reaction cell. (b) An epi-white light and epi-fluorescence image is acquired from the bottom of the microchannels in the reaction cell as detection and encoding image respectively in order to get the final assay result. (c) The schematic setup of a home-constructed inverted optical microscopic detection system.

Figure 2 | Zoom-in view of the recorded epi-white light image. The blue and green circle outlines the edge of the microchannel and bead respectively.

BMP format with a size of 2560 × 1920. And every bead is depicted by about 15000 pixels, which is enough for its characteristics recognition. In the epi-fluorescence image, different intensities of the beads represent different abundance of the target biomolecules. While in the epi-white image, the color codes of the beads represent the target species. Since the two modal images were acquired without changing the object position, the beads share the same coordinates in the two images, which lay the basis for the image alignment. Therefore, just by identifying the fluorescence intensity of the beads and retrieving their color code on the same position, whole multiplex assays can be interpreted.

Automated location and accurate boundary determination of PCBs. In the epi-white light image, the metal microchannel array has higher brightness and different color in comparison with beads, which is favorable to the extraction of beads. However, the margin of the microchannel was chamfered during the fabrication process. As can be seen from the zoom-in view in Fig. 2, the blue and green circle outlines the margin of the microchannel and bead respectively. And there is a relatively darker region between them with the color similar to that of the bead, which makes it difficult to determine the exact boundary between beads and microchannels. Hence, the epi-fluorescence image is processed firstly to extract the beads in our algorithm.

We have developed a novel extraction method that automatically extracts every intact bead in the epi-fluorescence image for multiplex assays. First, an adaptive enhancement is applied to the epi-fluorescence image, and then a statistical pattern recognition algorithm is utilized for the locating and extraction for the intact beads. This section describes the process in detail.

Segmentation is the process of distinguishing the beads from the background by setting an appropriate threshold and partitioning the image into two classes of pixels. However, in practical applications beads in the image will have various fluorescence intensities, those with high intensity of fluorescence will lighten the background around. In the histogram of the pixel intensities (Fig. 3 (a)), the pixels of the background and the beads overlap with each other in occurrence at lower intensity values, making it difficult to find an appropriate value for binarization. Classical algorithms such as the global threshold processing[27] and Otsu[28] method have been applied respectively. Nonetheless, they could not properly segment the beads, as illustrated in Fig. 3 (b) and (c).

Then an adaptive method is proposed and applied to increase the contract of the image, as seen in Fig. 3 (f). In comparison with the performances of the top-hat and the bottom-hat transformation (Fig. 3 (d) and (e)), not only the contrast is increased, but also the contour of every bead becomes clearer. Inspection of the histogram for the enhanced image reveals a 'dip' between the background peak and beads signals, and subsequent segmentation via Otsu method reveals excellent agreement with the boundaries of the beads (Fig. 3 (g)).

In order to proceed the subsequent data analysis, every bead in the epi-fluorescence image should be extracted separately with its boundary accurately determined. Furthermore, beads with incomplete or irregular shapes due to limit of the field view or manufacturing defect in the metal microarray channels should be removed as they will influence the quantified fluorescence intensities. Hence, we proposed a statistical pattern recognition algorithm to extract the position of every bead, and then utilized the statistical geometric features to classify these beads and exclude the defective ones. As seen from the area distribution of the beads (Fig. 4 (a)), it's obvious that most intact beads have relative larger areas above 10000. Hence, a threshold is setting to 10000 to screen the regions got above. If the area value of the certain region is larger than the threshold, it is regarded as an intact bead and retained; otherwise it is removed from the image. The result in Fig. 4 (b) shows all the beads left after the screening. Then the boundary of every extracted bead is obtained through using an opening operation and marked in different colors (Fig. 4 (c) and (d)). As seen from the epi-white light image (Fig. 4 (c)), the green contours outlines the accurate boundary of the beads.

Extracting the pixels that depict the bead accurately is a key step in the subsequent analysis, especially for the automated decoding of PCBs, as any errors incurred are bound to propagate through and influence the final results. As illustrated in Fig. 5, the performance of the as-proposed extraction method is directly compared with two other ones, the template matching algorithm based on fixed circle[29] and the adaptive shape method[30] based on watershed transformation, which are classical and widely used in gene detection for microarray images along with various gridding algorithms[31–33]. However, the microchannel array has a hexagonal arrangement, resulting in the vertical projection signals overlapping with each other. Hence, the gridding work is done line by line. As seen from the zoom-in view of (A1), (A2), (B1) and (B2), the blue lines describe the gridding results and every bead is extracted within the small block.
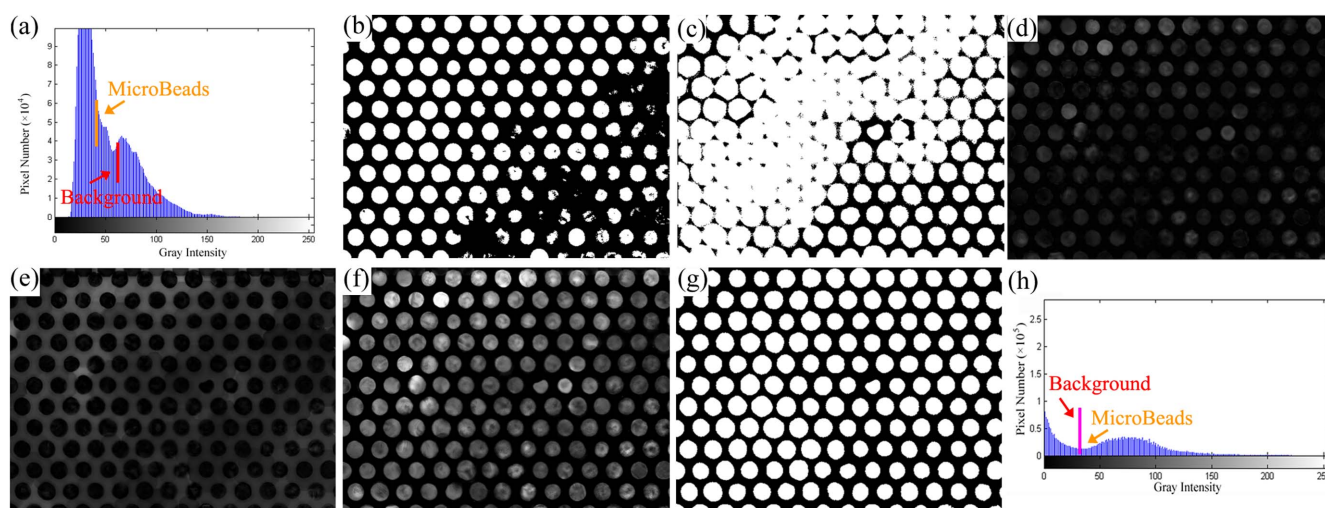

Figure 3 | Binarization of the epi-fluorescence images of PCBs array. (a) Histogram of the epi-fluorescence grayscale image. (b) Epi-fluorescence image binarized by using global threshold processing with a threshold of 57.25 and (c) Otsu method with a threshold of 27. Result of (d) top-hat transformation, (e) bottom-hat transformation, (f) adaptive enhancement, and (g) binarization of (f) via Otsu method. (h) Histogram of the grayscale image after enhancement. There's a 'dip' between the background peak and beads signals.
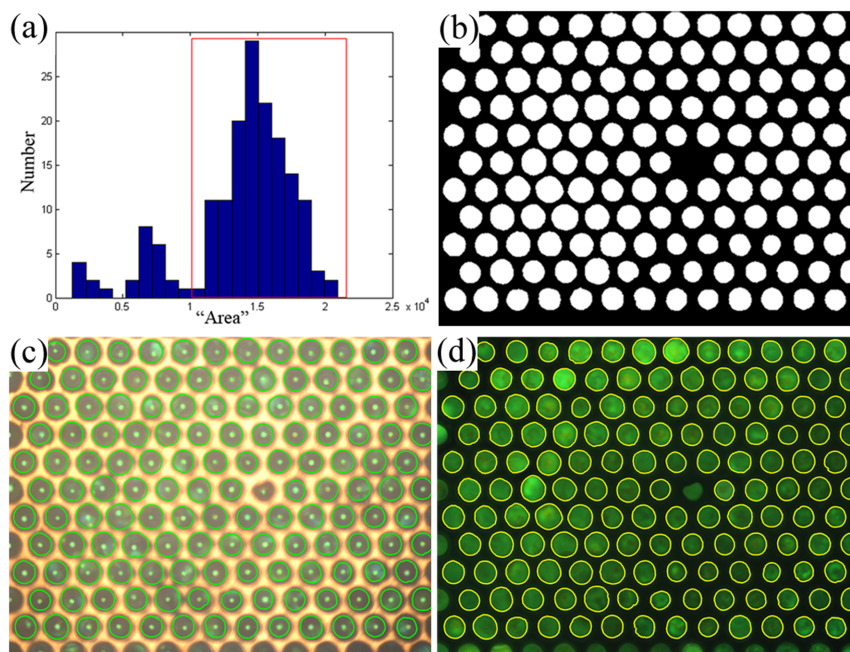
Figure 4 | Extraction of the PCBs array. (a) Area distribution of the beads. Most intact beads have areas lager than 10000. (b) Extracted Beads left after using a statistical pattern recognition algorithm. The incomplete and irregular beads have been excluded. Contours indict the extracted beads in (c) the epi-white light image and (d) the epi-fluorescence image.

Whereas, the fixed circle method only extracts a fixed circular edge for every bead, ignoring its variable size. This means that the fluorescence information of some relative larger beads is left out, while the background information is contained in some circles. Although the watershed method extracts an accurate edge that matches the bead, the defective one with incomplete shape is included in the result, as indicted by the red rectangle in (A2). And the marginal beads in (B2), which shouldn't be counted as the eventual objects for data analysis, are also extracted incorrectly due to the inaccurate gridding and reserved in this method. Therefore, the as-proposed extraction algorithm avoids the complicated calculation of the gridding work and automatically extracts all the intact beads. At the same time, accurate boundary is determined for every bead, as illustrated in (A3) and (B3). By using the method, the pixels of every intact bead could be

automatically obtained and then used as the basis to retrieve and identify the color codes on the same position in the epi-white light image.

Decoding of PCBs colors. The decoding of PCBs colors plays a vital role in realizing the multiplex assays. Beads with different color codes should be identified and classified into the corresponding categories. As RGB space is most commonly used in the storage of color images, it is thought that using the scatter plot of the intensities of RGB channels is an effective way to distinguish different colors, as they distribute separately with each other. For example, this method has been applied for the differential count of leukocytes[34], which utilizes the fluorescence intensities (red versus green) to differentiate the leukocyte subtypes. However, in the epi-white light image, the absolute intensities of color channels vary accordingly with the excitation source brightness or angle of illumination. Therefore, we proposed an approach based on the color ratiometric to eliminate influences of illumination. Because the intensities of RGB have similar variables under different illumination and the ratios change much smaller than the absolute intensities. By using the method, the RGB color space is transformed into the ratiometric color map shown in Fig. 6 (b). Different colors occupy different places in the map. As long as the ratios are specified, different color codes could be identified. We measured form 1500 beads and used the color ratiometric to classify these codes. Figure 6 (c) shows a scatter plot of the color ratiometric ($M(r)/M(g)$ versus $M(b)/M(g)$), where $M(r)$, $M(g)$ and $M(b)$ represent the mean values of the characteristic RGB colors inside the whole bead. In the scatter plot, each dot represents a detected bead and the recorded dots falling into four clusters describe four different color encodings. Every cluster is marked in a certain color corresponding to its code. However, the clusters overlap with each other, resulting in unsuccessful classification of different codes and wrong interpretation of the multiplex assays.

Figure 6 (d) shows another scatter plot of the color ratiometric ($C(r)/C(g)$ versus $C(b)/C(g)$) measured from the same beads, but processed using the characteristic value of RGB colors inside the bead instead of the mean value. The dots fall into four distinct clusters, which is easier to be distinguished. There are two main considera-
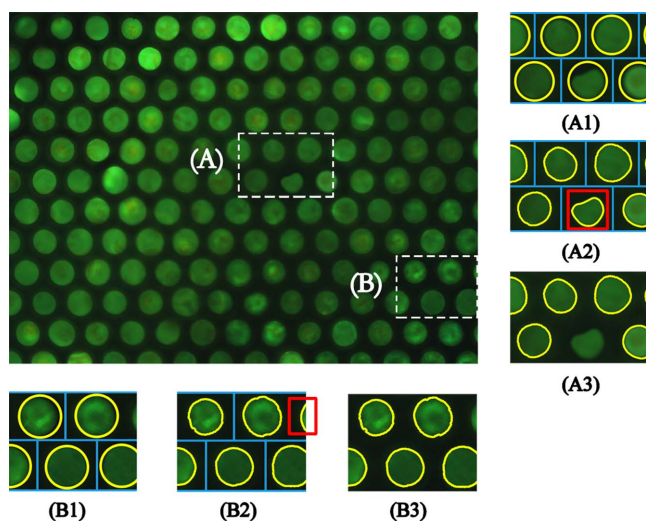

Figure 5 | Result of different extraction methods for PCBs array. (A1) and (B1) show the extraction of beads using fixed circle method. (A2) and (B2) show the extraction results using adaptive method. (A3) and (B3) shows the extraction result using the algorithm proposed in this paper.
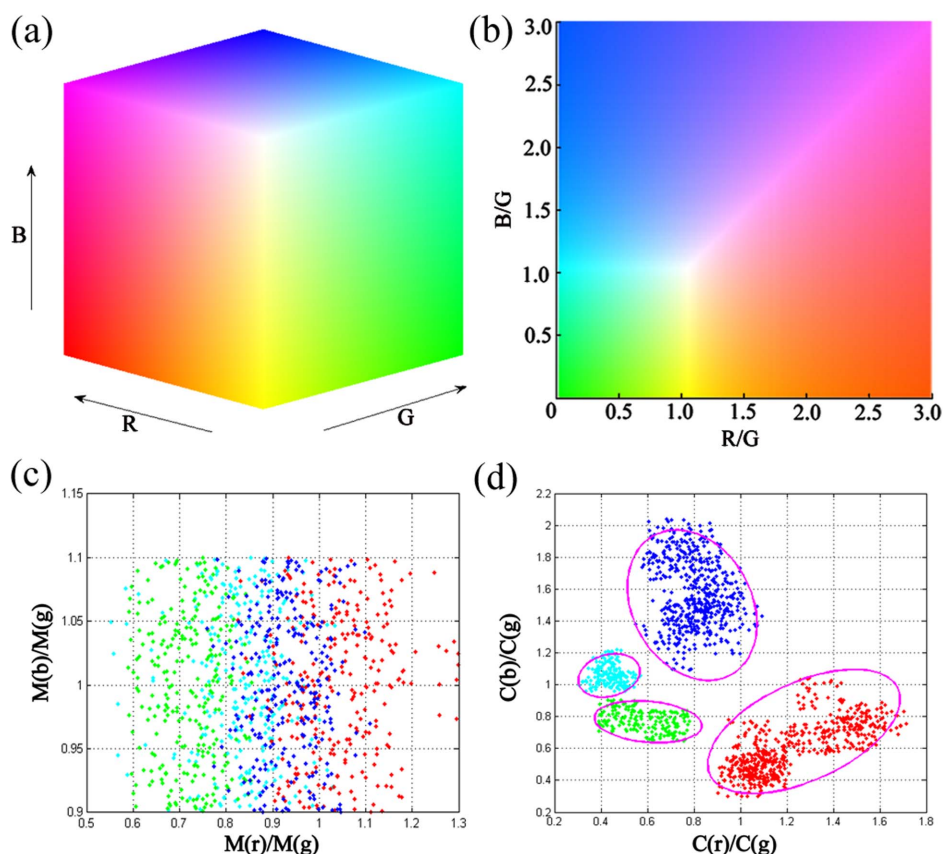
Figure 6 | Code identification of the PCBs array. (a) The RGB color space; (b) The ratiometric color map; $C(g)$ is set larger than 85 to guarantee that the maximum value of $C(r)/C(g)$ and $C(b)/C(g)$ are smaller than 3 and to limit the size of the map. (c) The scatter plot of the color ratiometric ($M(r)/M(g)$ versus $M(b)/M(g)$) determined by using the mean values of the color spots. (d) The scatter plot of the color ratiometric ($C(r)/C(g)$ versus $C(b)/C(g)$) measured from the same beads, but processed using the characteristic values of the color spots.

tions needed to be taken for better code identification. First, the bright color spot in the center of the bead represents the code and usually has higher intensity, but it only occupies a small part of the bead. While the other regions have much lower intensities and make no sense. Second, the mean value takes all the pixels inside the bead into calculation and could only depict the average color. But the characteristic value selects pixels with high intensities inside the spots and avoids the impact of other regions. Hence, the characteristic value fully represents the color characteristics of the beads. For an instance, dots of the orange and the blue codes occupy the bottom right cluster and the top cluster, respectively. These two clusters have a long distance with each other as the two codes have bigger difference in the components of red and blue. The cyan cluster adjoins the green cluster as the two codes have similar components of green and blue. The distribution of the clusters is in accordance with the color ratiometric shown in Fig. 6 (b).

Ellipses around each color cluster represent the approximated gating boundaries obtained by fitting a minimum volume enclosing ellipsoid (MVEE)[35] with an error rate of 10%, as shown in Fig. 6 (d). If a dot falls inside a certain ellipse, it means the bead has a color code the ellipse represents, otherwise regarded as an invalid bead. Beads presenting weak colors due to fabrication will not be identified a code, as they can't be recognized by human eyes. Some beads with normal colors also fall outside the ellipses in the experiment, but for the measured amount of 1500 beads in total, the inaccuracy is less than 10% and is acceptable. As there are no more than 200 beads within one image or even less in practical application, it implies that the decoding method is good enough to distinguish these color codes under the current configuration.

Discussion

When the PCBs are incorporated in microfluidic chips for POCT applications, lots of designs and forms may be adopted and unexpected situations may happen as well. In order to show the robustness of our bead extraction algorithm, we have also evaluated them on a set of images with different configurations. As shown in Fig. 7 (a), in an image of a microfluidic chip with rectangle microchannel array, the shape of the PCBs array varies a lot due to the non-uniform shape of the microchannel arrays and different size of PCBs. While in Fig. 7 (c), there were some microchannels not occupied by PCBs and the chip orientation was changed so that the PCBs distribute in an irregular way. In addition, the images were clipped into smaller sizes, which changed many size-related parameters.

Use of the as-proposed extraction method to process images taken under varied configurations revealed the results that were highly consistent, as seen from Fig. 7 (a)–(d). And other classical methods also have been tested on these images for comparisons. However, a tilt correction needs to be done firstly for rotated ROIs (Fig. 7 (c) and (d)) when using the classical gridding method. As illustrated in Fig. 7 (e) and (f), the valley value of the maximum energy spectrum density curve is utilized to correct the image and the gridding work is done according to the corrected projection signals. One limitation of this gridding method is that the iterative rotation of images is time-consuming, especially when the desired accuracy becomes higher. Furthermore, in the subsequent bead extraction, the size-related parameters become not appropriate and not applicable due to the variation of the microarrays, such as the grid division gaps used in the gridding method, the size and the shape of the templates used in the segmentation method, and so on. The red rectangles labeled in Fig. 7
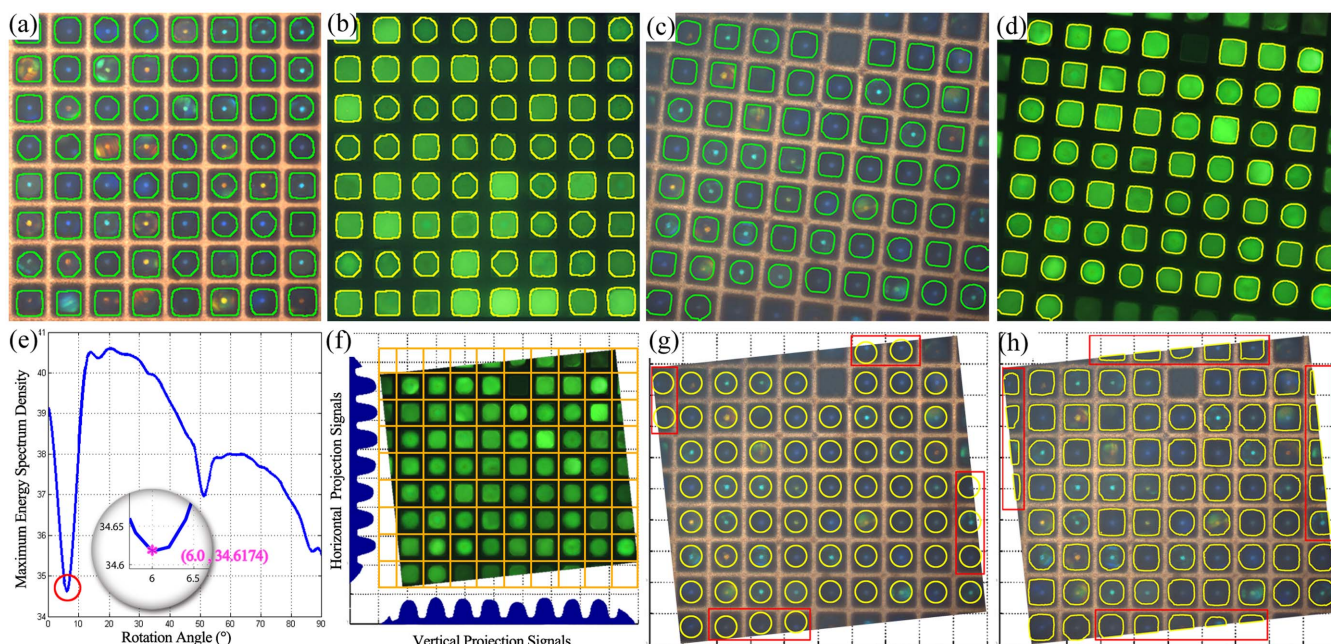
Figure 7 | Comparison of the bead extraction by as-proposed and classical methods. (a)–(d) The extraction results by using the as-proposed method under different configurations. (a) and (b) PCBs array in square microchannels arranged in squares. (c) and (d) PCBs array in square microchannels with some vacancies in rotated images. (e)–(h) The gridding and extraction results of (c) and (d) by using classical methods for comparison. (e) Tilt correction by using the maximum energy spectrum density of the vertical grayscale projection signals of (d). Inset is the zoom-in of the valley. The best rotation angle for tilt correction corresponds to the valley value. (f) Image of (d) after tilt correction by contrarotated 6° and then gridding according to the corrected horizontal and vertical projection signals. (g) and (h) Bead extraction by using fixed circle method and adaptive method, respectively. The red rectangles indicate the defective extractions.

(g) and (h) indicate the defective extractions by using fixed circle method and adaptive method, respectively. Hence, compared with these algorithms, the as-proposed extraction method possesses several advantages. First, it averts the gridding work along with the related influences and increases the efficiency of the algorithm. Second, it owns a good pertinence to intact beads and could exclude the defective ones. Third, this method results in consistent extraction result even under different configurations. Hence, this extraction method possesses a strong robustness without any need of manual parameter adjustment to accomplish the analysis, providing a guarantee for the automated decoding of PCBs array for multiplex assays.

In the process of PCBs array decoding, the characters of PCBs and the optical detection system imposed great difficulties. On the one hand, the structure colors derived from Bragg reflection of photonic crystal are angle-dependent[19,26], which means that different colors will be observed when viewed from different angles especially on curved bead surface. Therefore, the beads in the image present iridescent color instead of pure one. For example, the beads with orange codes often present yellow, orange and green color simultaneously. While the green beads also show cyan color within the same bead. These similar colors overlap with each other and decrease the accuracy in decoding. On the other hand, due to the size variation of beads and microchannels, not all the beads are in the same focal plane, which explains why the beads have spots with varied brightness and size in the center. Beads with low brightness will decrease the color intensities presented in the image. And the varied sizes of the color spots also increase the complexity in extracting the color characters for decoding.

Transforming the RGB color into another color space, such as HSI or HSV, is an alternative way to recognize different colors, as the hue is determined by the location of the peak in the spectral distribution[36]. However, it is not capable of distinguishing these colors due to the influence of the iridescent color, especially when the colors are similar. At the same time, large amount of transformations will

greatly reduce the speed of the system. Hence, our work presents a novel and effective strategy by using color ratiometric.

We take the image in Fig. 7 (a) and (b) for an instance to evaluate the accuracy of the decoding method for different color codes and the edge of extracted bead in the image is marked with corresponding color, as shown in Fig. 8. It can be seen that all the beads in the image are identified correctly as their real codes except for two beads, B and C. As in the zoom-in views on the right of Fig. 8, the two beads marked in white edges both have very weak color spots due to the defect of fabrication quality. Although the two beads have complete shapes and are extracted, the characteristic values of the two beads are [98.6000, 116.6000, 117.7000] and [85.4000, 95.9000, 99.1000],
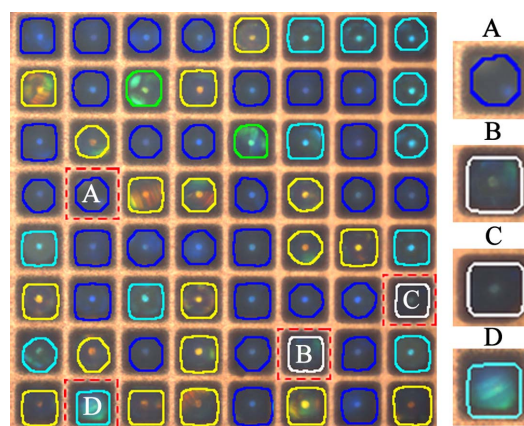

Figure 8 | Result of the code identification. Beads with different color codes are marked in corresponding color. Bead A shows that the color spot lies in the bottom right instead of in the center, while bead D shows a color region instead of a color spot for decoding. The two beads B and C marked white represent the unidentified color code.
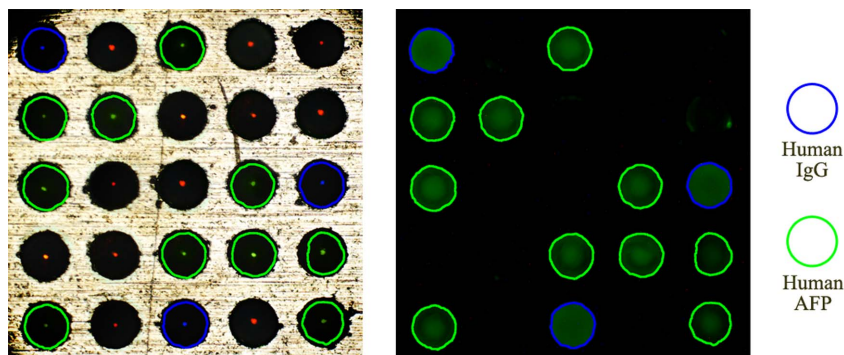
Figure 9 | Image decoding result of a multiplex protein assay. Blue and green circle represent codes for Human IgG and Human AFP, respectively.

respectively, which are very similar to gray color. And their color cannot be decoded neither by our strategy nor human eyes.

In addition, the central location doesn't coincide exactly with the color spot in most instances. As seen from the zoom-in view of the bead A in Fig. 8, the blue spot lies in the bottom right of the bead. If we only extract the color of the central part, the result may be another unrecognized bead. While the identification algorithm proposed extracts the characteristic color within the whole bead and don't suffer from the variations of the color spots. In the case that the bead D presents, there's just a color region instead of a color spot, and the algorithm still performs well. These results demonstrate that the proposed method of color decoding is more appropriate for the analysis of the image based on microfluidic chip.

In order to demonstrate the effectiveness of our image decoding methods in practical applications under various situations, a multiplex protein detection experiment is performed and analyzed with 190 μm PCBs and 150 μm metal microchannels, of which the result is shown in Fig. 9. In the reaction cell, there is goat anti-human IgG, mouse anti-human β2-MG and mouse anti-human AFP immobilized on blue, red and green encoded beads respectively. Yet, the introduced sample solution only contains human IgG and human AFP. Therefore, red encoded PCBs work as control. It is showed that in the epi-fluorescence image, although there's background fluorescence signals like in the column 4, row 2 microchannel, our algorithm successfully extracts 13 intact PCBs that need to be decoded after sandwich immunoreactions. And then the beads on the same positions in the epi-white light images are identified with a color code, as can be seen that 3 blue and 10 green encoded are circled with blue and green circles respectively. Although some beads present dim colors like that in column 1, row 2 and 5, their characteristic colors are extracted successfully and correctly. And the result shows intuitively that there are only two kinds of protein, human IgG and human AFP, in the sample solution. The fluorescence intensities of them after background correction are 35.4471 and 26.5828 respectively, which can be used for the subsequent concentration analysis. All these procedures are done automatically in seconds for efficient and proper deciphering of the multiplex protein assay.

In summary, this paper proposed an automated decoding method for the microfluidic chip based on PCBs array to realize the multiplex assays. By using this method, every intact bead in the image is accurately extracted and decoded under various configurations in practical applications. And no high accuracy instruments or user-interaction is needed, which contributes to the development of high-throughput bioassay and portable and intelligent detection system based on the PCBs, especially in POCT.

Methods

Fabrication of microfluidic chip with PCBs array. The microfluidic chip was assembled from two glass slides, two PDMS slabs and six metal microchannel array plates. In the PDMS slab, there are six steel tubing as inlet or outlet connected to six through holes of 2 mm. Six metal microchannel array plates with diameter of 3 mm were sandwiched between through holes of two PDMS slabs (Fig. 1 (a)). And the PDMS slabs were sealed with glass slides and the through holes form reaction cells. The PCBs were injected into the reaction cells with a syringe and trapped in the microchannel array plates.

Inverted optical microscopic detection system. In brief, the detection system employs coaxial illumination for both white light and fluorescence. It consists of a CCD camera (QImaging RETIGA EXi), an objective (Olympus UMPlan Fl 10×), a metal halide lamp (MEJIRO GENOSSEN, 200 W), a dichroic mirror (Thorlabs), a tube lens (Thorlabs) and two Stepper-Motor-Driven Filter Wheels (Thorlabs) with a 458 nm–492 nm excitation filter and a 510 nm–550 nm emission filter respectively, which can be switched on and off to capture epi-fluorescence images and epi-white light images.

Image analysis. To remove the thermal noise in the image caused by imaging equipment[37], a morphological opening operation is adopted. Then an adaptive enhancement algorithm is proposed and applied to increase the contract of the image. Suppose the fluorescence grayscale image is represented as $f(x,y)$, then the whole procedure to enhance the image is expressed in equation (1).

$$f_E(x,y) = f(x,y) + f_T(x,y) - f_B(x,y) \tag{1}$$

Where $f_E(x,y)$ represents the enhanced image, $f_T(x,y)$ and $f_B(x,y)$ represent the top-hat and the bottom-hat transformation, respectively. Subsequently, the enhanced image is segmented via the Otsu method.

In order to exclude the beads with incomplete or irregular shapes, we adopt a statistical pattern recognition algorithm, which utilize a unicom domain extraction method based on the 8-neighbour structure[38] to extract every bead as an independent region in the image. Then the number of pixels in every unicom domain is calculated as its 'area'. The 'area' is considered as a criterion to classify these beads and exclude the defective ones. The intact beads typically generate larger 'area' values, while those of the defective ones are distributed broadly among the lower values. An appropriate threshold is set according to the feature of the statistical distribution. When the area value of the certain region is larger than the threshold, it's regarded as an intact beads and it's retained, otherwise removed from the image.

A novel approach based on ratiometric instead of absolute intensity measurements is proposed on the basis of the extraction results to identify different color codes. It operates as follows: the characteristic value of color red (C(r)) is calculated as equation (2) and so are C(g) and C(b).

$$C(r) = \frac{\sum_{i=1}^{N} I(r)_i}{N} \tag{2}$$

Where $I(r)_i$ is the i-th largest red intensity of pixels inside the bead, but they are all required below 250 to rule out singular values. The value of N is set as 20 in the experiment and remains constant when analyzing different particles. Then the data in the ratiometric scatter plot (C(r)/C(g) versus C(b)/C(g)) is fit by a minimum volume enclosing ellipsoid, with an error rate of 10%. If a dot falls inside the ellipse, it means the bead owns the corresponding color code.

The image acquisition and the automatic image analysis were realized in Visual Studio 2010 with OpenCV 2.4.3.

Multiplex assays. A standard sandwich fluorescence immuoassays were adopted in the multiplex assays of protein. In brief, blue, red and green color encoded PCBs were immobilized with goat anti-human IgG, mouse anti-human β2-MG and mouse anti-human AFP respectively and trapped by the metal microchannel array in the microfluidic chip. Then 50 μL sample solution containing 10 μg/mL Human IgG and AFP was introduced into the reaction cells by a syringe pump with velocity of 50 μL/h at room temperature and washed with 1% BSA PBST buffer. After reacting with 10 μg/mL FITC tagged secondary antibodies (goat anti-

human IgG-FITC, mouse anti-human β2-MG-FITC and mouse anti-human AFP-FITC) and another washing, epi-fluorescence and epi-white images of PCBs array were captured.

1. Linder, V. Microfluidics at the crossroad with point-of-care diagnostics. *Analyst* **132**, 1186–1192 (2007).
2. Cheng, X. *et al.* A microfluidic device for practical label-free CD4+ T cell counting of HIV-infected subjects. *Lab Chip* **7**, 170–178 (2007).
3. Dimov, I. K. *et al.* Integrated microfluidic array plate (iMAP) for cellular and molecular analysis. *Lab Chip* **11**, 2701–2710 (2011).
4. Chin, C. D., Linder, V. & Sia, S. K. Commercialization of microfluidic point-of-care diagnostic devices. *Lab Chip* **12**, 2118–2134 (2012).
5. Guo, F. *et al.* A droplet-based, optofluidic device for high-throughput, quantitative bioanalysis. *Anal. Chem.* **84**, 10745–10749 (2012).
6. Tüdös, A. J., Besselink, G. A. & Schasfoort, R. B. Trends in miniaturized total analysis systems for point-of-care testing in clinical chemistry. *Lab Chip* **1**, 83–95 (2001).
7. Chin, C. D., Linder, V. & Sia, S. K. Lab-on-a-chip devices for global health: past studies and future opportunities. *Lab Chip* **7**, 41–57 (2007).
8. Weigl, B., Domingo, G., LaBarre, P. & Gerlach, J. Towards non-and minimally instrumented, microfluidics-based diagnostic devices. *Lab Chip* **8**, 1999–2014 (2008).
9. Gervais, L. & Delamarche, E. Toward one-step point-of-care immunodiagnostics using capillary-driven microfluidics and PDMS substrates. *Lab Chip* **9**, 3330–3337 (2009).
10. Luppa, P. B., Müller, C., Schlichtiger, A. & Schlebusch, H. Point-of-care testing (POCT): Current techniques and future perspectives. *TrAC, Trends Anal. Chem.* **30**, 887–898 (2011).
11. Zhu, H., Isikman, S. O., Mudanyali, O., Greenbaum, A. & Ozcan, A. Optical imaging techniques for point-of-care diagnostics. *Lab Chip* **13**, 51–67 (2013).
12. Zhao, X., Zhao, Y. & Gu, Z. Advances of multiplex and high throughput biomolecular detection technologies based on encoding microparticles. *Sci. China Chem.* **54**, 1185–1201 (2011).
13. Vignali, D. A. A. Multiplexed particle-based flow cytometric assays. *J. Immunol. Meth.* **243**, 243–255 (2000).
14. Gunderson, K. L. *et al.* Decoding Randomly Ordered DNA Arrays. *Genome Res.* **14**, 870–877 (2004).
15. Nolan, J. P. & Sklar, L. A. Suspension array technology: evolution of the flat-array paradigm. *Trends Biotechnol.* **20**, 9–12 (2002).
16. Cunin, F. *et al.* Biomolecular screening with encoded porous-silicon photonic crystals. *Nat. Mater.* **1**, 39–41 (2002).
17. Stoermer, R. L., Sioss, J. A. & Keating, C. D. Stabilization of silver metal in citrate buffer: barcoded nanowires and their bioconjugates. *Chem. Mater.* **17**, 4356–4361 (2005).
18. Stoermer, R. L. & Keating, C. D. Distance-dependent emission from dye-labeled oligonucleotides on striped Au/Ag nanowires: effect of secondary structure and hybridization efficiency. *J. Am. Chem. Soc.* **128**, 13243–13254 (2006).
19. Zhao, X. *et al.* Colloidal crystal beads as supports for biomolecular screening. *Angew. Chem. Int. Ed.* **45**, 6835–6838 (2006).
20. Wei, Q. *et al.* Fluorescent Imaging of Single Nanoparticles and Viruses on a Smart Phone. *ACS Nano* **7**, 9147–9155 (2013).
21. Navruz, I. *et al.* Smart-phone based computational microscopy using multi-frame contact imaging on a fiber-optic array. *Lab Chip* **13**, 4015–4023 (2013).
22. Ayas, S., Cupallari, A., Ekiz, O. O., Kaya, Y. & Dana, A. Counting Molecules with a Mobile Phone Camera Using Plasmonic Enhancement. *ACS Photonics* **1**, 17–26 (2014).
23. Feng, S. *et al.* Immunochromatographic Diagnostic Test Analysis Using Google Glass. *ACS Nano* **8**, 3069–3079 (2014).
24. Ozcan, A. Mobile phones democratize and cultivate next-generation imaging, diagnostics and measurement tools. *Lab Chip* **14**, 3187–3194 (2014).
25. Yang, Y. H., Buckley, M. J. & Speed, T. P. Analysis of cDNA microarray images. *Brief Bioinform.* **2**, 341–349 (2001).
26. Takeoka, Y. Angle-independent structural coloured amorphous arrays. *J. Mater. Chem.* **22**, 23299–23309 (2012).
27. Gonzalez, R. C., Woods, R. E. & Eddins, S. L. *Digital image processing using MATLAB.* (Publishing House of Electronics Industry, Beijing, China, 2009).
28. Otsu, N. A threshold selection method from gray-level histograms. *Automatica* **11**, 23–27 (1975).
29. Leung, Y. F. & Cavalieri, D. Fundamentals of cDNA microarray data analysis. *Trends Genet.* **19**, 649–659 (2003).
30. Yang, Y. H., Buckley, M. J., Dudoit, S. & Speed, T. P. Comparison of methods for image analysis on cDNA microarray data. *J. Comput. Graph. Stat.* **11**, 108–136 (2002).
31. Katzer, M., Kummert, F. & Sagerer, G. Methods for automatic microarray image segmentation. *IEEE Trans. Nanobiosci.* **2**, 202–214 (2003).
32. Brändle, N., Bischof, H. & Lapp, H. Robust DNA microarray image analysis. *Mach. Vision. Appl.* **15**, 11–28 (2003).
33. Blekas, K., Galatsanos, N. P., Likas, A. & Lagaris, I. E. Mixture model analysis of DNA microarray images. *IEEE Trans. Med. Imaging.* **24**, 901–909 (2005).
34. Shi, W., Guo, L., Kasdan, H. & Tai, Y. C. Four-part leukocyte differential count based on sheathless microflow cytometer and fluorescent dye assay. *Lab Chip* **13**, 1257–1265 (2013).
35. Kumar, P. & Yildirim, E. A. Minimum-Volume Enclosing Ellipsoids and Core Sets. *J. Optimiz. Theory. App.* **126**, 1–21 (2005).
36. Wang, X. Y., Wang, T. & Bu, J. Color image segmentation using pixel wise support vector machine classification. *Pattern Recogn.* **44**, 777–787 (2011).
37. Schena, M. *Microarray analysis.* (Wiley-Liss Hoboken, NJ, 2003).
38. Sonka, M., Hlavac, V. & Boyle, R. *Image processing, analysis, and machine vision.* (Cengage Learning, 2014).

Author contributions

J.Y., X.Z. and Z.G. wrote the main manuscript text. J.Y. and X.Z. designed and analyzed the experiments. X.W. made the PCBs and microfluidic chips and carried out the multiplex bioassays. All authors reviewed the manuscript.

Additional information

Competing financial interests: The authors declare no competing financial interests.

How to cite this article: Yuan, J., Zhao, X., Wang, X. & Gu, Z. Image Decoding of Photonic Crystal Beads Array in the Microfluidic Chip for Multiplex Assays. *Sci. Rep.* **4**, 6755; DOI:10.1038/srep06755 (2014).